ACS APPLIED MATERIALS & INTERFACES

Research Article

Cite This: ACS Appl. Mater. Interfaces 2018, 10, 35571−35579

www.acsami.org

Electrostatically Charged MoS_2/Graphene Oxide Hybrid Composites for Excellent Electrochemical Energy Storage Devices

Mao-Cheng Liu,*[,†] Yan Xu,[†] Yu-Xia Hu,[‖] Qing-Qing Yang,[†] Ling-Bin Kong,[†] Wen-Wu Liu,[†] Wen-Jun Niu,[†] and Yu-Lun Chueh*[,†,§,⊥]

[†]State Key Laboratory of Advanced Processing and Recycling of Non-Ferrous Metals and School of Materials Science and Engineering, Lanzhou University of Technology, Lanzhou 730050, P. R. China

[§]Department of Materials Science and Engineering and [‖]Frontier Research Center on Fundamental and Applied Sciences of Matters, National Tsing Hua University, Hsinchu 30013, Taiwan, ROC

[⊥]Department of Physics, National Sun Yet-Sun University, Kaohsiung 80424, Taiwan, ROC

Supporting Information

ABSTRACT: We demonstrate, for the first time, a new method of fabricating hybrid MoS_2/poly(ethyleneimine)-modified graphene oxide (PEI-GO) composites assembled through electrostatically charged interaction between the negatively charged MoS_2 nanosheets and positively charged PEI-GO in an aqueous solution. The GO can not only improve the electronic conductivity of the MoS_2/PEI-GO composites, leading to an excellent charge-transfer network, but also hamper the restacking of MoS_2 nanosheets. The composition ratios between MoS_2 and PEI-GO were also optimized with the highest specific capacitance of 153.9 F g^{-1} where 96.0% of the initial specific capacitance remains after 6800 cycles. The specific capacitance of only 117.5 F g^{-1} was observed for the pure MoS_2 nanosheets, and 68.2% of the initial specific capacitance was achieved after 5000 cycles. The excellent electrochemical performance of the hybrid MoS_2/PEI-GO composites was demonstrated by establishing an asymmetric supercapacitor with a MoS_2/PEI-GO-based negative electrode and an activated-carbon positive electrode. The asymmetric supercapacitor provided a maximum capacitance of 42.9 F g^{-1}, and 93.1% of the initial capacitance was maintained after 8000 cycles. Furthermore, a MoS_2/PEI-GO//activated-carbon asymmetric supercapacitor delivered an energy density of 19.3 W h kg^{-1} and a power density of 4500 W kg^{-1}, indicating the potential of the hybrid MoS_2/PEI-GO composites in electrochemical energy storage applications.

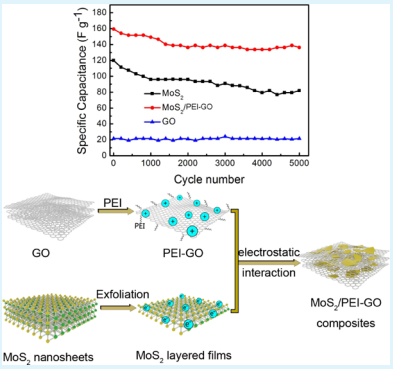

KEYWORDS: *MoS_2/PEI-GO composites, exfoliation, opposite charge, supercapacitor, electrostatically charged interaction*

INTRODUCTION

Because of the limited availability of fossil fuels and deteriorating ecological environment, developing equipment with excellent energy storage is important.[1−4] Among all energy storage devices, supercapacitors, namely electrochemical capacitors, have been studied extensively. This is because supercapacitors possess a higher power density with a longer cycle life than batteries.[5−8] Depending on the charge storage mechanism, supercapacitors can be classified into two types, pseudocapacitors and electrical double-layer capacitors (EDLCs). For the pseudocapacitor, the electrical energy is stored through a reversible faradic reaction by using typical electrode materials such as conducting polymers and transition metal oxides.[9−12] In the EDLC, the charge storage depends on ion adsorption and desorption processes, for which the electrodes are typically made of porous carbon materials.[13] The electrode material is the most important factor in determining the properties of the EDLC. In recent years, transition metal dichalcogenides, the typical two-dimensional materials with unique electrical and mechanical properties, have attracted considerable attention as electrode materials for supercapacitors.[14]

As a prototypical transition metal dichalcogenide material, MoS_2 has been widely applied in a variety of fields.[14−18] Compared with graphene structures that feature a single layer of carbon atom, the MoS_2 possesses a "sandwich" structure, comprising a three-atom layer based on S−Mo−S, a three-layer structure with sulfur atoms in two hexagonal planes divided by a plane of molybdenum atoms, and molybdenum and sulfur atoms with valence states of 4+ and 2−, respectively. Because this structure is analogous to graphene, MoS_2 is a potential supercapacitive material with a high theoretical specific capacitance.[19−21] Krishnamoorthy et al. reported that a chemically prepared MoS_2 nanostructure has a capacitance of 92.85 F g^{-1}.[22] Huang et al. synthesized MoS_2 nanosheets as electrode materials with a specific capacitance of up to 129.2 F g^{-1} and the capacitance retention of 85.1% after 500 cycles.[23]

Received: June 1, 2018
Accepted: August 28, 2018
Published: August 28, 2018

DOI: 10.1021/acsami.8b09085
ACS Appl. Mater. Interfaces 2018, 10, 35571−35579

MoS_2 can be synthesized to have various morphologies and provide the high specific capacitance. However, the relatively low electronic conductivity of MoS_2 severely limits its electrochemical performance. Therefore, several researchers have combined MoS_2 with other conducting materials for improving its electronic conductivity and capacitance performance. For example, Sun et al. fabricated three-dimensional graphene/MoS_2 by using a one-pot hydrothermal approach, which achieved a specific capacitance of 410 F g^{-1} at 1 A g^{-1}.[24] Bissett et al. fabricated a MoS_2/graphene hybrid film with a capacitance of 11 mF cm^{-2} at 5 mV s^{-1}.[25] Although its electrical conductivity can be improved, the restacking of MoS_2 restricts its electrochemical properties. However, one of the most versatile methods for layered films is electrostatic self-assembly in aqueous solutions. The technique has recently been used to prepare hybrid electroactive films. Yu et al. and Li et al. obtained poly(ethyleneimine)-modified graphene nanosheet/multi-walled nanotube−COOH films and PDDS/poly(sodium 4-styrenesulfonate)-mediated graphene sheets/poly(diallyldimethylammonium chloride) MnO_2 sheets through electrostatic self-assembly, respectively, for which both of them exhibited excellent properties as electrodes for supercapacitors.[26,27]

In this regard, we, for the first time, demonstrated PEI-modified GO nanosheets combined with the negatively charged exfoliated-MoS_2 nanosheets through electrostatically charged interaction, thus, forming hybrid MoS_2/PEI-GO composites. Furthermore, the different compositional ratios between MoS_2 and GO were optimized. The hybrid MoS_2/PEI-GO composites as electrodes exhibited the highest specific capacitance of 153.9 F g^{-1} at 1 A g^{-1} and a strong cycling performance with 96.0% of the initial capacitance was maintained after 6800 cycles, which were superior to the properties of the MoS_2 electrode. Moreover, a MoS_2/PEI-GO//activated-carbon (AC) asymmetrical supercapacitor achieved a high-power density with an excellent cycling stability. The results indicate that the hybrid MoS_2/PEI-GO composites are promising materials for the supercapacitor.

EXPERIMENTAL SECTION

Materials. Analytically pure $Na_2MoO_4{\cdot}2H_2O$, CH_4N_2S, hexane, and GO were acquired from Sinopharm Chemical Reagent Co. Ltd. *N*-Butyl-lithium (2.5 mol L^{-1} in hexane) and poly(ethyleneimine) were purchased from Aladdin Industrial Corporation. A poly(vinylidene fluoride) (PVDF) membrane was purchased from Merck Millipore Ltd.

Synthesis of Hybrid MoS_2/PEI-GO Composites. The hybrid MoS_2/PEI-GO composites were fabricated through the following process. First, MoS_2 was synthesized through a facial hydrothermal method. Subsequently, 5 mmol of $Na_2MoO_4{\cdot}2H_2O$ and 20 mmol CH_4N_2S were added to deionized water with 60 mL, and the mixed solution was then dumped in an autoclave at 200 °C for 24 h. After the reaction was completed, the products were rinsed with water and ethanol four times and then dried in an oven at 60 °C for 12 h, yielding MoS_2 powder. The MoS_2 powder was chemically exfoliated through lithium intercalation where 10 mL of butyl-lithium was added to 0.3 g of MoS_2 powder under argon conditions, followed by magnetic stirring performed at reflux for 48 h.[28] The mixture was filtered through a PVDF membrane and washed repeatedly using hexane. Then, the intercalated MoS_2 was dispersed in deionized water with ultrasonication for 1 h, yielding a concentration of 2 mg mL^{-1} with the ζ-potential of −34.9 mV. The GO dispersion was diluted to form a solution with a concentration of 0.25 mg mL^{-1}. The resulting 100 mL homogeneous GO dispersion (with a ζ-potential of −52.7 mV) was mixed with 100 mL of poly(ethyleneimine) solution (4 mg mL^{-1}) and stirred at 60 °C for 12 h. The liquid was centrifuged to remove excess polymers and then dispersed in deionized water to form a solution of 0.25 mg mL^{-1} PEI-modified GO nanosheets with a ζ-potential of 37.2 mV. Finally, the negatively charged MoS_2 nanosheets (200 mg) were mixed with the positively charged PEI-GO nanosheets (25 mg) under strong stirring. The mixed solution was then centrifuged and dried to obtain the hybrid MoS_2/PEI-GO composites (with a ζ-potential of −3.0 mV). For comparison, exfoliated-MoS_2 layered films and GO nanosheets without PEI were simply mixed to obtain MoS_2/GO composites. In addition, composites with high concentrations of MoS_2 layered films (HCMoS_2/PEI-GO) and high concentrations of PEI-GO nanosheets (MoS_2/HCPEI-GO) were also prepared.

Structure and Electrochemical Characterization. Preparation and characterization of working electrodes and asymmetric supercapacitors, and relevant material characterization are described in the Supporting Information.

RESULTS AND DISCUSSION

To confirm the structures of the exfoliated-MoS_2 layered films and hybrid MoS_2/PEI-GO composites, X-ray diffraction (XRD) and Raman measurements were performed. Figure 1a displays the XRD spectra of the exfoliated-MoS_2 and the hybrid MoS_2/PEI-GO composites. Clearly, the peaks of (002), (100), (003), and (110) planes were observed in the XRD pattern of the exfoliated MoS_2, confirming 2H-phase MoS_2 (JCPDS No. 37-1492).[22,28−31] The strongest peak at 14.2° is due to the (002) plane of the MoS_2 nanosheets attributable to the stacking of the S−Mo−S layer, namely a two-dimensional layered structure.[32] However, as can be seen in the XRD spectra of hybrid MoS_2/PEI-GO composites, the peaks almost disappeared due to (002) and (110) planes of MoS_2 nanosheets, indicating that the crystal structure of MoS_2 nanosheets was destroyed once combining with GO nano-

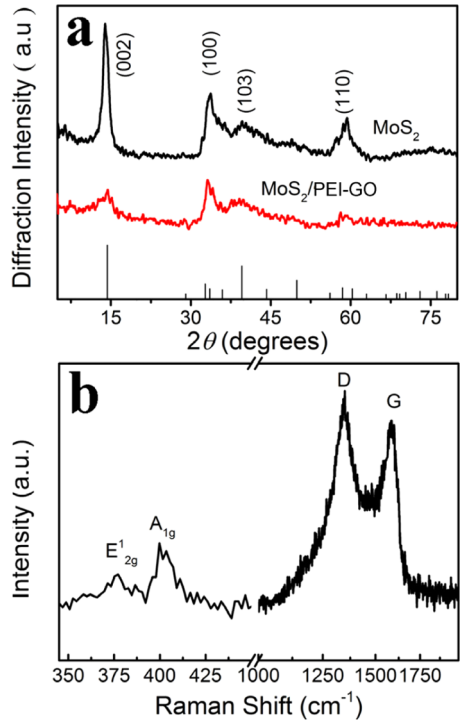

Figure 1. (a) XRD results of the MoS_2 nanosheets and hybrid MoS_2/PEI-GO composites. (b) Raman spectra of the hybrid MoS_2/PEI-GO composites.

DOI: 10.1021/acsami.8b09085
ACS Appl. Mater. Interfaces 2018, 10, 35571−35579

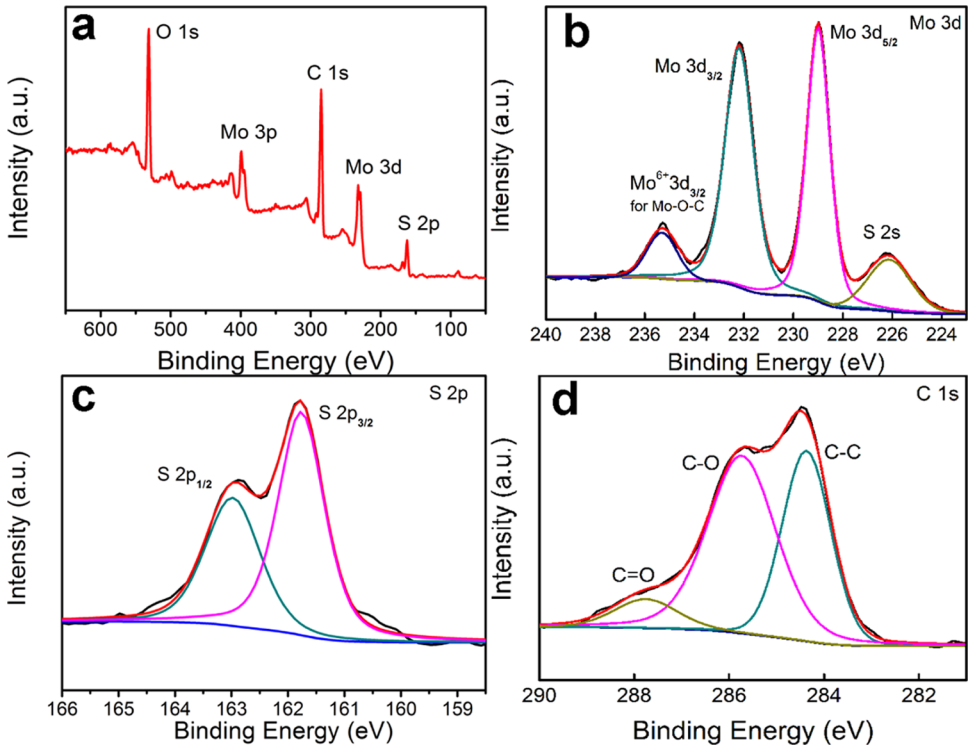

Figure 2. (a) Overall XPS, (b) Mo 3d, (c) S 2p, and (d) C 1s XPS spectra of hybrid MoS_2/PEI-GO composites.

sheets.[33] The results indicated that the MoS_2 nanosheets were successfully exfoliated into a small number of layers and anchored on GO nanosheets. In addition, the primary peak of the GO due to the (001) plane was not observed. This is because the amount of GO nanosheets is small, and it is thus covered by exfoliated-MoS_2 layered films.[34,35] The combination of exfoliated-MoS_2 layered films and GO nanosheets was further investigated using the Raman spectra as shown in Figure 1b. The Raman spectra of hybrid MoS_2/PEI-GO composites exhibited two characteristic peaks located at 1349 and 1589 cm^{-1}, corresponding to D and G bands of GO, respectively. The D band is attributed to the vibrations of carbon atoms corresponding to the defects and disorder in carbon materials whereas the G band is related to the crystalline graphite. The intensity ratio of the D band to the G band (I_D/I_G) is an indication of defects in the carbon lattice.[26] The I_D/I_G value was evaluated according to the whole peak areas under D and G bands. The I_D/I_G value for hybrid MoS_2/PEI-GO composites was further calculated to be 1.31, which is higher than that of the GO nanosheets (normally, 1.2) as shown in Figure S1. Therefore, the introduction of the exfoliated-MoS_2 layered films can result in more edges and defects on the hybrid MoS_2/PEI-GO composites. This not only facilitates ion diffusion but also provides more active sites for electrochemical reactions. Moreover, two other distinct peaks located at 383 and 402 cm^{-1} were observed, which agreed closely with the E_{2g} and A_{1g} modes of MoS_2. Typically, the E_{2g} mode can be attributed to the in-layer displacement of Mo and S atoms, whereas the A_{1g} mode was due to the out-of-layer symmetric displacements of S atoms. Thus, the hybrid MoS_2/PEI-GO composites were successfully prepared.

X-ray photoelectron spectroscopy (XPS) was performed to investigate the elements and valence state information of the hybrid MoS_2/PEI-GO composites as shown in Figure 2. As can be seen in Figure 2a, the elements of O, Mo, S, and C were clearly identified in the hybrid MoS_2/PEI-GO composites. The O element was derived from surface adsorption because the sample was exposed to air. Figure 2b shows Mo 3d spectra where two characteristic peaks at 228.9 and 232.2 eV correspond to the Mo $3d_{5/2}$ and Mo $3d_{3/2}$ orbitals, respectively, indicating the presence of Mo^{4+}. In addition, a peak was observed at approximately 235.3 eV, possibly due to the partial oxidation of MoS_2 at the edges and defects, which is attributed to molybdenum (Mo^{6+}) in an octahedral configuration. The high-resolution S 2p spectrum revealed that peaks located at 161.7 eV for S $2p_{3/2}$ and 162.9 eV for S $2p_{1/2}$ are traits of S^{2-} as shown in Figure 2c. The results were in accordance with those expected for MoS_2. The C 1s spectrum exhibited three peaks, which corresponded to the sp^3 hybrid C (C−C, 284.5 eV), the hydroxyl C (C−O, 285.9 eV) and the epoxy C (C═O, 287.8 eV), respectively (Figure 2d).[26] As a result, detailed compositional analyses of the XPS spectra demonstrated that the MoS_2 nanosheets were successfully combined with GO nanosheets.

The morphologies and microstructures of the samples were analyzed through scanning electron microscopy (SEM) and transmission electron microscopy (TEM). Figure 3a shows the typical SEM images of the MoS_2 nanosheets. The MoS_2 nanosheets exhibited tightly interlaced flakes, forming an interconnected nanostructure. After the MoS_2 nanosheets were further exfoliated into small pieces, the crystallinity of MoS_2 was destroyed (Figure 3b). The exfoliated-MoS_2 layered films were anchored on GO nanosheets through electrostatic interactions, forming alternating layers of the hybrid MoS_2/PEI-GO composites (Figure 3c). The corresponding TEM images further reveal the morphology and structural characteristics of MoS_2 nanosheets, exfoliated-MoS_2 nanosheets, and hybrid MoS_2/PEI-GO composites are shown in Figure 3d−f, respectively. The TEM image of MoS_2 layered films shown in Figure 3d indicates that the average flake size is approximately 50 nm with a thickness of approximately 20 nm. The inset in

DOI: 10.1021/acsami.8b09085
ACS Appl. Mater. Interfaces 2018, 10, 35571−35579

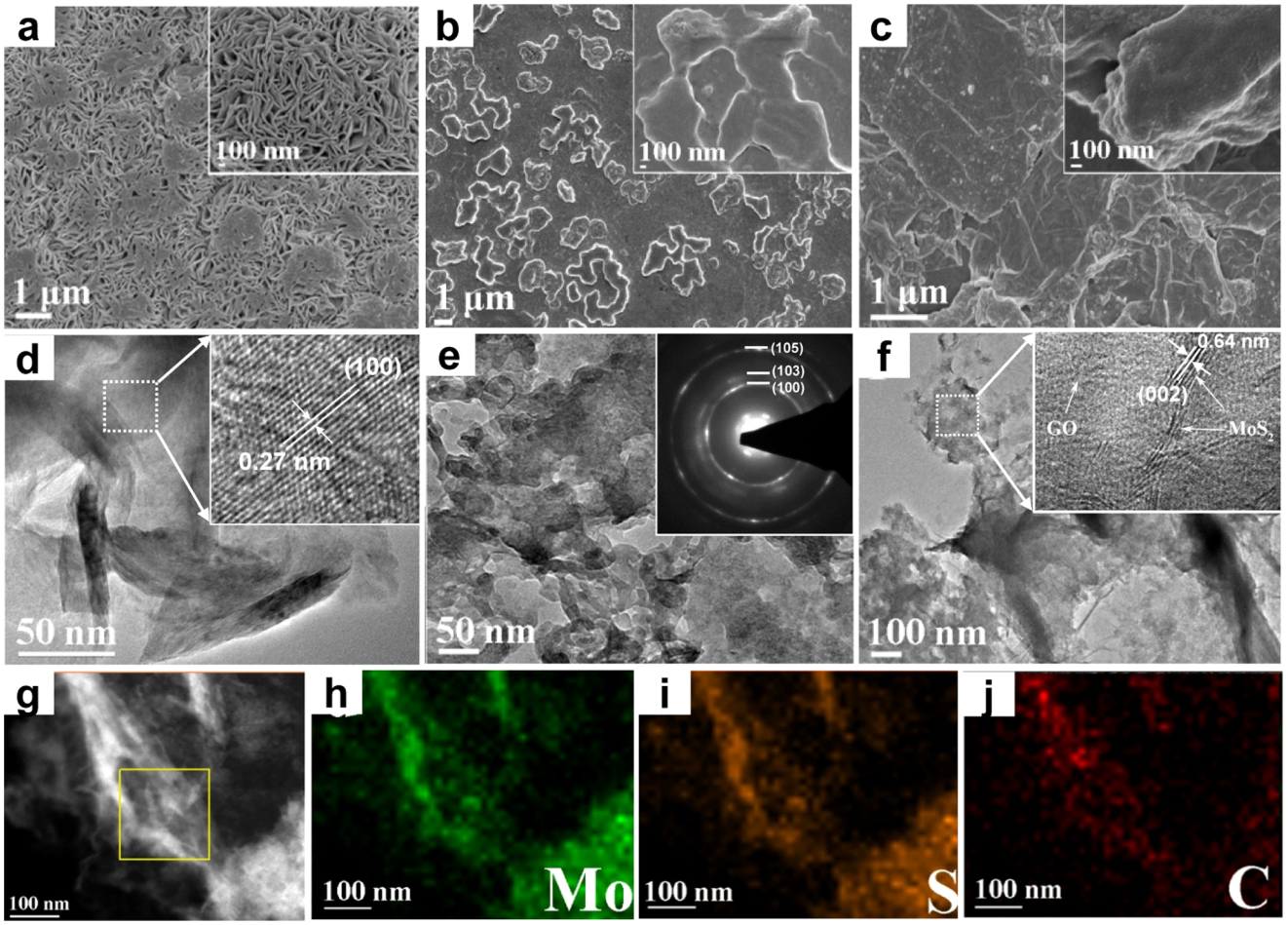

Figure 3. (a–c) SEM images of the MoS_2 nanosheets, the exfoliated-MoS_2 layered films and the hybrid MoS_2/PEI-GO composites. (d–f) TEM images of the MoS_2 nanosheets, the exfoliated-MoS_2 layered films and the hybrid MoS_2/PEI-GO composites. Insets show the high-resolution TEM image of the MoS_2 nanosheets, selected diffraction patterns of the exfoliated-MoS_2 layered films, and the high-resolution TEM image of the hybrid MoS_2/PEI-GO composites. (g) A TEM image of the hybrid MoS_2/PEI-GO composites with different element mapping images, including (h) Mo, (i) S, and (j) C, respectively.

Figure 3d shows a high-resolution TEM (HRTEM) image of the MoS_2 nanosheets, where the plane of (100) with an internal spacing of 0.27 nm can be indexed, revealing evidence of the crystal structure. Figure 3e shows the TEM image of the MoS_2 nanosheets after further exfoliation process and the corresponding selected diffraction pattern (SAD) with indexed-planes of (100), (103), and (105) matching the MoS_2 phase was confirmed. The ring patterns from the SAD confirmed much smaller grain sizes of MoS_2 nanosheets after the further exfoliation process. The TEM image of the hybrid MoS_2/PEI-GO composites in Figure 3f distinctly reveals exfoliated-MoS_2 layered films anchored on the curled GO nanosheets. The inset shows the corresponding HRTEM image of the hybrid MoS_2/PEI-GO composites where the MoS_2 layered structure with an internal spacing of 0.64 matching the (002) plane along the *C* axis was indexed. In addition, the predominance of areas with dark fringes and small corrugated areas are evident. The corrugated areas were large and curled GO nanosheets while the dark fringes were associated with the folded edges of the exfoliated-MoS_2 layered films.[36] The layered structure of the hybrid MoS_2/PEI-GO composites provided abundant channels for electrolyte transportation. The appearance and distribution of the exfoliated-MoS_2 layered films exposed on the surface of the GO nanosheets were visualized using energy-dispersive X-ray spectroscopy, which was used to create elemental maps of Mo, S, and C as shown in Figure 3g–j. The results further demonstrated the uniform distribution of exfoliated-MoS_2 layered films and GO nanosheets together. Such intimate surface-to-surface contact can not only hamper the restacking of exfoliated-MoS_2 layered films for ensuring high cycling stability but also facilitate fast and stable electron and ion transport.[37] Figure S2 presents the thermogravimetric curve of MoS_2/PEI-GO composites measured at an air atmosphere to verify the GO content. The results indicate that the GO content in the MoS_2/PEI-GO composites is 10.1%.

Figure 4a shows the typical cyclic voltammetry (CV) curves of the MoS_2 nanosheets at different scan rates. No redox peaks were observed in the CV curves, and the shape was almost rectangular, indicating an ideal capacitive behavior, which is in agreement with the results from the previous report.[22] The CV curves maintained their rectangular shape with increasing scan rates, revealing rapid electron and ion transport at a large scan rate. The galvanostatic charge–discharge (GCD) curves of the MoS_2 nanosheets were investigated at varying current densities (Figure 4b). Using eq S1, the specific capacitances were calculated to be 117.5, 102, 92.7, 85.1, and 79.3 F g^{-1} at the current densities of 1, 2, 3, 4, and 5 A g^{-1}, respectively (Figure

DOI: 10.1021/acsami.8b09085
ACS Appl. Mater. Interfaces 2018, 10, 35571–35579

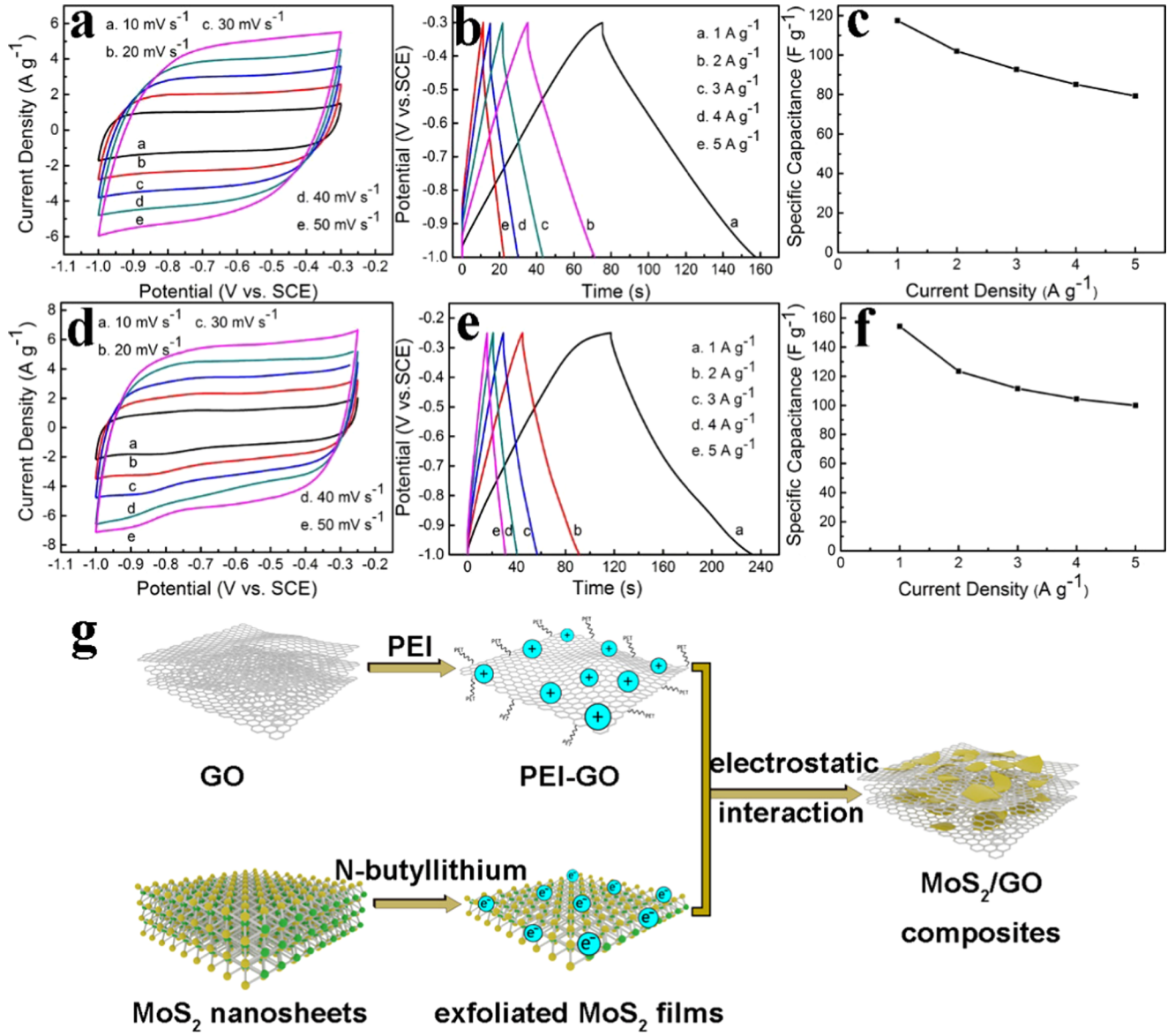

Figure 4. (a) CV and (b) GCD curves of the MoS_2 nanosheets, (c) Specific capacitance of the MoS_2 nanosheets at different current densities, (d) CV and (e) GCD curves of hybrid MoS_2/PEI-GO composites, (f) Specific capacitance of hybrid MoS_2/PEI-GO composites at different current densities. (g) Schematic illustration of self-assemble between MoS_2 and PEI-GO.

4c). Thus, approximately 67% of the initial value for the current density changed from 1 to 5 A g^{-1}. The charge−discharge curves are symmetric, revealing an ideal supercapacitive behavior. Despite the high reversibility and rate capability, the specific capacitance is still poor due to the inferior electrical conductivity and tightly packed structure. To overcome this problem, the MoS_2 nanosheets were further exfoliated into small pieces and anchored on GO nanosheets through electrostatic interactions, thereby forming alternating layers of the hybrid MoS_2/PEI-GO composites. The rectangular nature of the CV curves in Figure 4d indicates that the hybrid MoS_2/PEI-GO electrodes exhibit an ideal capacitive behavior. This is because the hybrid MoS_2/PEI-GO composites efficiently hampered the aggregation and restacking of MoS_2 nanosheets, thus providing fast and stable ion transport to improve the capacitance.[38] In addition, the deviation from rectangular shape can be attributed to the presence of 1T MoS_2 during exfoliation.[39] The adding of GO nanosheets accelerated electron transport during the charging−discharging process and improved the rate capability.[40] The CV curves maintained their initial shape at a large scan rate of 50 mV s^{-1}, indicating a high rate capability. The GCD curves at various current densities are shown in Figure 4e. The hybrid MoS_2/PEI-GO electrodes exhibited a typical isosceles triangle shape, indicating the ideal capacitor behavior. The specific capacitances of the MoS_2/PEI-GO electrode calculated from the discharge time were 153.9, 123.5, 111.6, 104.5, and 100 F g^{-1}, corresponding to the current densities of 1, 2, 3, 4, and 5 A g^{-1}, respectively (Figure 4e). The specific capacitance of the MoS_2/PEI-GO is slightly lower than some previously reported MoS_2/GO composites prepared by other methods, such as layered MoS_2/graphene composites (243 F g^{-1} at a discharge current density 1 A g^{-1}),[41] three-dimensional MoS_2/graphene aerogel composites (268 F g^{-1} at a discharge current density 0.5 A g^{-1}),[42] MoS_2/graphene hybrid films (282 F g^{-1} at a scan rate of 20 mV s^{-1}),[43] and so on. However, the study

DOI: 10.1021/acsami.8b09085
ACS Appl. Mater. Interfaces 2018, 10, 35571−35579

still proves a new way to fabricate MoS_2- and GO-based intercalation composites by electrostatic attraction between the negatively charged MoS_2 nanosheets and positively charged PEI-GO in an aqueous solution. This self-assembled process is also available for the synthesis of other intercalation materials. Figure 4f shows that 65% specific capacitance was retained when the current density increased from 1 to 5 A g^{-1}. Obviously, the hybrid MoS_2/PEI-GO composites exhibit the higher specific capacitance with the excellent rate capability than that of the MoS_2 nanosheets. The prominent properties are due to the fact that the negatively charged MoS_2 few layers were tightly anchored on positively charged PEI-GO nanosheets through electrostatic interaction up to saturation, thus hampering the restacking of MoS_2 layered films and improving the conductivity as schematically illustrated in Figure 4g.

To prove that the hybrid MoS_2/PEI-GO composites are the optimal sample, the electrochemical characterization of MoS_2/GO, HCMoS_2/PEI-GO, and MoS_2/HCPEI-GO was performed and is shown in Figure S3. The specific capacitance of MoS_2/GO is 81.3 F g^{-1} at 1 A g^{-1} and is far less than the hybrid MoS_2/PEI-GO composites, whereas the specific capacitances of HCMoS_2/PEI-GO and MoS_2/HCPEI-GO is 152.2 and 148.5 F g^{-1} at a current density of 1 A g^{-1}, respectively, indicating that the composites fabricated through the electrostatic interaction exhibit prominent electrochemical performance. Meanwhile, the construction of composites does not change anymore after the saturation of charge adsorption. Therefore, the specific capacitances of the hybrid MoS_2/PEI-GO composites are almost the same as HCMoS_2/PEI-GO and MoS_2/HCPEI-GO. Figure 5a shows Nyquist plots of the electrodes in a frequency range from 10^{-1} to 10^5 Hz. The plots comprise a semicircular part in the high-frequency region and a linear part in the low-frequency region. The inset shows an equivalent circuit fitted with the spectroscopy curve, and the suitable parameters for different components acquired using the Zswinpwin software package are shown in Table 1. The

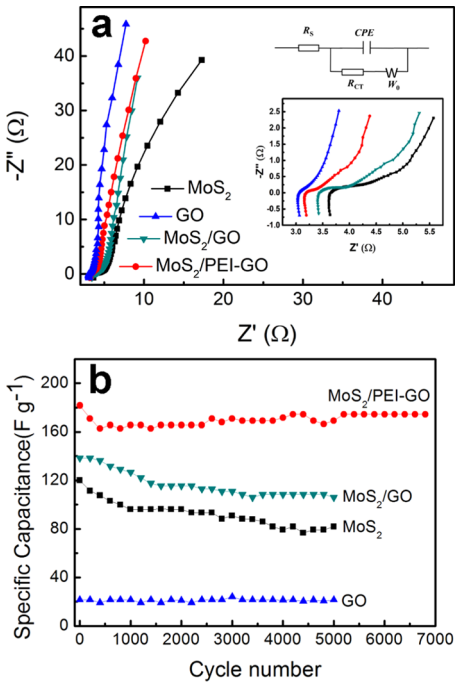

Figure 5. (a) Nyquist plots of MoS_2 nanosheets, GO, MoS_2/GO, and hybrid MoS_2/PEI-GO composites. Insets (1) and (2) show the semicircle at high frequency and equivalent circuit, respectively. (b) Cycling performance of MoS_2, GO, MoS_2/GO, and MoS_2/PEI-GO at a current density of 2 A g^{-1}.

Table 1. Shows Fitted Parameters for Nyquist Plots Obtained by the Zswinpwin Software at Different Samples

sample	R_S (Ω)	R_{CT} (Ω)	W_0 ($S{\cdot}s^{-0.5}$)
MoS_2	3.615	0.01	0.024
GO	2.986	0.002	0.004
MoS_2/GO	3.356	0.0024	0.031
MoS_2/PEI-GO	3.194	0.0039	0.034

equivalent circuit comprises a series resistance (R_S), charge-transfer resistance (R_{CT}), Warburg resistance (W_0), and double-layer capacitance (CPE). The R_{CT} of the hybrid MoS_2/PEI-GO composites (0.0039 Ω) is lower than that of MoS_2 nanosheets (0.01 Ω), indicating the rapid electron transport during the electrochemical reactions and the excellent rate capability. In addition, impedance plots in the low-frequency region were all subvertical, indicating a relatively low Warburg resistance. The W_0 of the hybrid MoS_2/PEI-GO composites (0.024 $S{\cdot}s^{-0.5}$) is lower than that of the MoS2 nanosheets (0.034 $S{\cdot}s^{-0.5}$), indicating that the alternative layered structure of the hybrid MoS_2/PEI-GO composites can accelerate ion transport and provide superior capacitance. GCD measurements were performed at 2 A g^{-1} as shown in Figure 5b. Clearly, the specific capacitance of the hybrid MoS_2/PEI-GO composites remains at approximately 96.0% after 6800 cycles, indicating favorable cycling stability. However, the cycling performance of the MoS_2 and MoS_2/GO electrodes was inferior with only 68.2 and 76.6% of the specific capacitance maintained after 5000 cycles. Evidently, the cycling stability of the hybrid MoS_2/PEI-GO composites was superior to that of the MoS_2 electrode. The improved supercapacitive properties of the hybrid MoS_2/PEI-GO composites were attributed to the incorporation of the GO to accelerate electron transfer due to their high electrical conductivity and anchoring the exfoliated-MoS_2 layered films on the GO nanosheets to form an alternating layered structure with high stability and integrity, which is favorable for improving the cycling stability, hindering the aggregation and restacking of MoS_2 and were favorable for the rapid diffusion of ions.

To investigate the electrochemical performance of the hybrid MoS_2/PEI-GO composites in practical applications, an asymmetric supercapacitor was developed with an AC mode as a positive electrode and the hybrid MoS_2/PEI-GO composites as a negative electrode. The accessed voltage window was determined to be 1.8 V as shown in Figure S4. Figure 6a shows the CV curves of asymmetric supercapacitors in potential window ranges of 0−1.8 V. No redox peaks were observed in the CV curves, indicating the ideal capacitor behavior. Moreover, the CV curves retained a rectangular shape at a high scan rate (100 mV s^{-1}), indicating the excellent reversibility of the asymmetric supercapacitor. The GCD curves of the asymmetric supercapacitor at different current densities are shown in Figure 6b, for which a linear and triangular shape can be obtained, indicating an ideal capacitive behavior. The specific capacitances as shown in Figure 6c were determined to be 42.9, 39.7, 35.8, 32.6, 30, and 27.5 F g^{-1} at the current densities of 0.5, 1, 2, 3, 4 and 5 A g^{-1}, respectively. These capacitances resulted in an outstanding rate capability of

DOI: 10.1021/acsami.8b09085
ACS Appl. Mater. Interfaces 2018, 10, 35571−35579

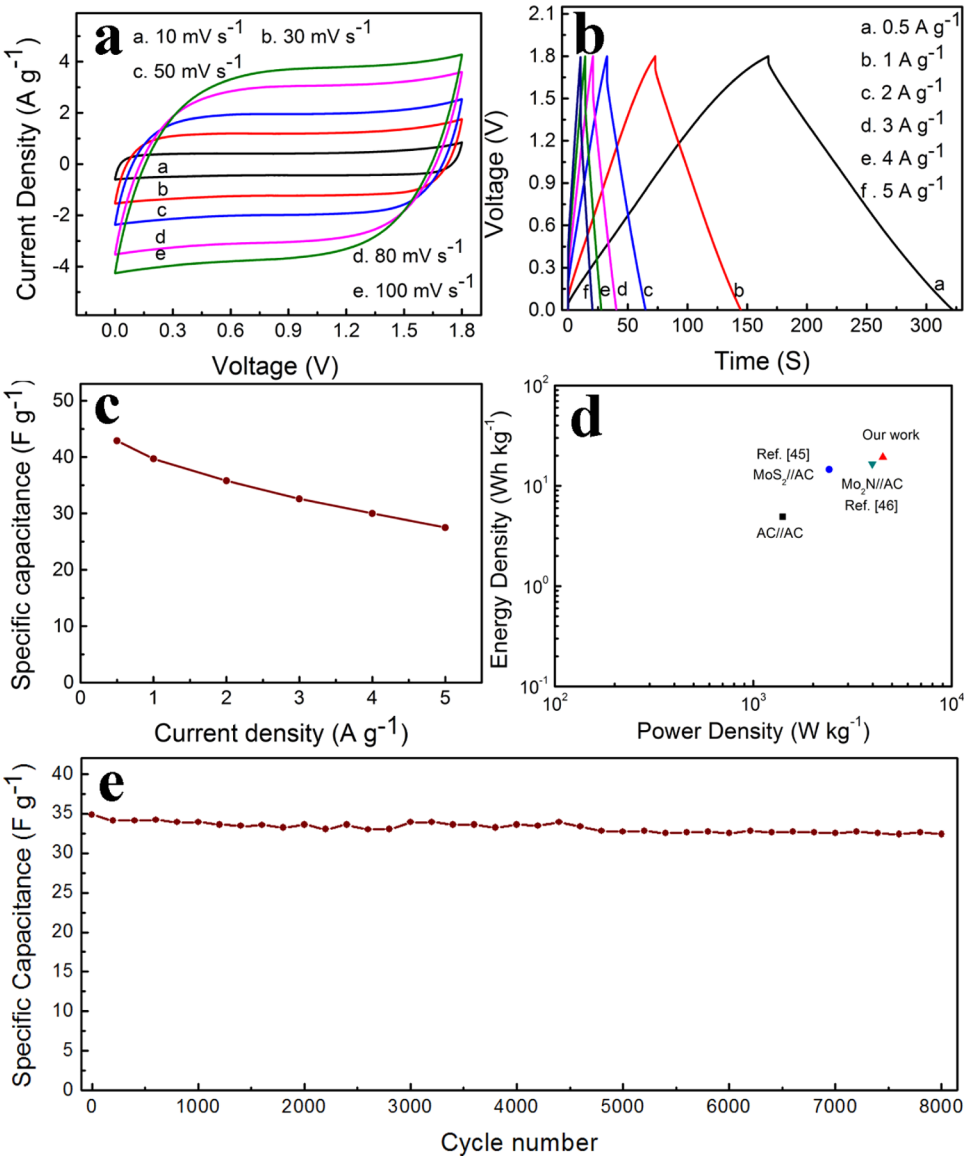

Figure 6. Electrochemical performance of the MoS_2/PEI-GO//AC asymmetric supercapacitor: (a) CV curves, (b) GCD curves, (c) specific capacitances vs current density curves, (d) Ragone plots, (e) cycling performance.

64% with the current density increasing from 0.5 to 5 A g^{-1}. Figure 6d lists the comparison of different material systems at energy density as the function of power density from the literature. Distinctly, the hybrid MoS_2/PEI-GO composite-based asymmetric supercapacitor delivered an energy density of 19.3 W h kg^{-1} and a power density of 4500 W kg^{-1}. The MoS_2/PEI-GO//AC supercapacitor provided the energy density and the power density higher than those of an AC//AC supercapacitor and those reported in the literature.[42,43] In addition, the cycling performance of the MoS_2/PEI-GO//AC supercapacitor is shown in Figure 6e. The specific capacitance of the MoS_2/PEI-GO//AC supercapacitor remained at 93.1% after 8000 cycles, indicating the steady cycling ability. It also exhibited a remarkable electrochemical reversibility and practical energy densities, indicating that the hybrid MoS_2/PEI-GO composites are potential electrode materials for supercapacitors.[44,45]

CONCLUSIONS

In summary, exfoliated-MoS_2 films were anchored on GO nanosheets through electrostatically charged interaction, thus forming the hybrid MoS_2/PEI-GO composites as a potential electrode material for high-performance supercapacitors. The highest specific capacitance at the optimized hybrid MoS_2/PEI-GO composites of 8−1 being 153.9 F g^{-1} with 65% capacitance maintained at 5 A g^{-1} can be obtained. Moreover, the hybrid MoS_2/PEI-GO composites exhibited superior cycling stability with the capacitance retention of 96.0% after 6800 cycles. The excellent capacitive behavior was attributed to fast electron transport due to the addition of GO and alternative layers favorable for ion transport. Furthermore, a MoS_2/PEI-GO//AC asymmetric supercapacitor delivered an energy density of 19.3 W h kg^{-1} and a power density of 4500 W kg^{-1}, indicating the potential of the hybrid MoS_2/PEI-GO composites in electrochemical energy storage applications. This study inspires a new method for improving the electrochemical properties of other transition metal sulfides for supercapacitors.

DOI: 10.1021/acsami.8b09085
ACS Appl. Mater. Interfaces 2018, 10, 35571−35579

■ ASSOCIATED CONTENT

Supporting Information

The Supporting Information is available free of charge on the ACS Publications website at DOI: 10.1021/acsami.8b09085.

Preparation and characterization of working electrodes and asymmetric supercapacitors; relevant material characterization; Raman spectra of GO nanosheets; CV and GCD curves of the MoS_2/GO composites, the HCMoS_2/PEI-GO composites and the MoS_2/HCPEI-GO composites; CV curves of the AC and the hybrid MoS_2/PEI-GO composites at a scan rate of 50 mV s^{-1}; galvanostatic charge−discharge curves of the AC and the hybrid MoS_2/PEI-GO composites; cyclic voltammogram curves of the MoS_2/PEI-GO//AC asymmetric supercapacitor at different operation voltages with a scan rate of 20 mV s^{-1} (PDF)

■ AUTHOR INFORMATION

Corresponding Authors

*E-mail: liumc@lut.cn (M.-C.L.).
*E-mail: ylchueh@mx.nthu.edu.tw (Y.-L.C.).

ORCID

Ling-Bin Kong: 0000-0002-2271-4202
Yu-Lun Chueh: 0000-0002-0155-9987

Notes

The authors declare no competing financial interest.

■ ACKNOWLEDGMENTS

This work was supported by the National Natural Science Foundation of China (No. 21403099) and the Natural Science Funds for Distinguished Young Scholars of Gansu Province (No. 1606RJDA320). In addition, this research is also supported by the Ministry of Science and Technology through grant through grants no. 107-2923-E-007-002-MY3, 107-2112-M-007-030-MY3, 106-2923-E-007-006-MY2, 105-2119-M-009-009, and 107-3017-F-007-002 and the National Tsing Hua University through Grant no. 105A0088J4. Y.-L.C. greatly appreciates the use of the facility at CNMM.

■ REFERENCES

(1) Wei, L.; Sevilla, M.; Fuertes, A. B.; Mokaya, R.; Yushin, G. Polypyrrole-Derived Activated Carbons for High-Performance Electrical Double-Layer Capacitors with Ionic Liquid Electrolyte. *Adv. Funct. Mater.* **2012**, *22*, 827−834.

(2) Chen, H.; Cong, T. N.; Yang, W.; Tan, C.; Li, Y.; Ding, Y. Progress in Electrical Energy Storage System: A Critical Review. *Prog. Nat. Sci.: Mater. Int.* **2009**, *19*, 291−312.

(3) Zhang, L.; Han, P.; Wang, K.; Lu, Z.; Wang, L.; Zhu, Y.; Zhang, Q. Enhanced luminescence of Sr_2SiO_4:Dy^{3+} by sensitization (Ce^{3+}/Bi^{3+}) and its composition-induced phase transition. *J. Alloys Compd.* **2012**, *541*, 54−59.

(4) Sun, T.-M.; Dong, L.-M.; Wang, C.; Guo, W.-L.; Wang, L.; Liang, T.-X. Effect of Porosity on the Electrical Resistivity of Carbon Materials. *New Carbon Mater.* **2013**, *28*, 349−354.

(5) Feng, M.; Du, Q.; Su, L.; Zhang, G.; Wang, G.; Ma, Z.; Gao, W.; Qin, X.; Shao, G. Manganese Oxide Electrode with Excellent Electrochemical Performance for Sodium Ion Batteries by Pre-Intercalation of K and Na Ions. *Sci. Rep.* **2017**, *7*, No. 2219.

(6) Wen, Q.; Kong, F.; Ren, Y.; Cao, D.; Wang, G.; Zheng, H. Improved Performance of Microbial Fuel Cell through Addition of Rhamnolipid. *Electrochem. Commun.* **2010**, *12*, 1710−1713.

(7) Islam, M. S.; Fisher, C. A. Lithium and Sodium Battery Cathode Materials: Computational Insights into Voltage, Diffusion and Nanostructural Properties. *Chem. Soc. Rev.* **2014**, *43*, 185−204.

(8) Kötz, R.; Carlen, M. Principles and Applications of Electrochemical Capacitors. *Electrochim. Acta* **2000**, *45*, 2483−2498.

(9) Dong, X.; Guo, Z.; Song, Y.; Hou, M.; Wang, J.; Wang, Y.; Xia, Y. Flexible and Wire-Shaped Micro-Supercapacitor Based on Ni(OH)2-Nanowire and Ordered Mesoporous Carbon Electrodes. *Adv. Funct. Mater.* **2014**, *24*, 3405−3412.

(10) Chaikittisilp, W.; Hu, M.; Wang, H.; Huang, H. S.; Fujita, T.; Wu, K. C.; Chen, L. C.; Yamauchi, Y.; Ariga, K. Nanoporous Carbons through Direct Carbonization of a Zeolitic Imidazolate Framework for Supercapacitor Electrodes. *Chem. Commun.* **2012**, *48*, 7259−7261.

(11) Rakhi, R. B.; Chen, W.; Cha, D.; Alshareef, H. N. Substrate Dependent Self-Organization of Mesoporous Cobalt Oxide Nanowires with Remarkable Pseudocapacitance. *Nano Lett.* **2012**, *12*, 2559−2567.

(12) Chen, H.; Fan, M.; Li, C.; Tian, G.; Lv, C.; Chen, D.; Shu, K.; Jiang, J. One-Pot Synthesis of Hollow NiSe−CoSe Nanoparticles with Improved Performance for Hybrid Supercapacitors. *J. Power Sources* **2016**, *329*, 314−322.

(13) Wang, Y.; Shen, C.; Niu, L.; Li, R.; Guo, H.; Shi, Y.; Li, C.; Liu, X.; Gong, Y. Hydrothermal Synthesis of CuCo2O4/CuO Nanowire Arrays and RGO/Fe2O3 Composites for High-Performance Aqueous Asymmetric Supercapacitors. *J. Mater. Chem. A* **2016**, *4*, 9977−9985.

(14) Huang, X.; Zeng, Z.; Zhang, H. Metal Dichalcogenide Nanosheets: Preparation, Properties and Applications. *Chem. Soc. Rev.* **2013**, *42*, 1934−1946.

(15) Hu, Z.; Wang, L.; Zhang, K.; Wang, J.; Cheng, F.; Tao, Z.; Chen, J. MoS2 Nanoflowers with Expanded Interlayers as High-Performance Anodes for Sodium-Ion Batteries. *Angew. Chem., Int. Ed.* **2014**, *53*, 12794−12798.

(16) Tan, C.; Zhang, H. Two-Dimensional Transition Metal Dichalcogenide Nanosheet-Based Composites. *Chem. Soc. Rev.* **2015**, *44*, 2713−2731.

(17) Chang, K.; Geng, D.; Li, X.; Yang, J.; Tang, Y.; Cai, M.; Li, R.; Sun, X. Ultrathin MoS2/Nitrogen-Doped Graphene Nanosheets with Highly Reversible Lithium Storage. *Adv. Energy Mater.* **2013**, *3*, 839−844.

(18) Hong, X.; Liu, J.; Zheng, B.; Huang, X.; Zhang, X.; Tan, C.; Chen, J.; Fan, Z.; Zhang, H. A Universal Method for Preparation of Noble Metal Nanoparticle-Decorated Transition Metal Dichalcogenide Nanobelts. *Adv. Mater.* **2014**, *26*, 6250−6254.

(19) Chang, K.; Chen, W.; Ma, L.; Li, H.; Huang, F.; Xu, Z.; Zhang, Q.; Lee, J.-Y.; Li, H. Graphene-Like MoS2/Amorphous Carbon Composites with High Capacity and Excellent Stability as Anode Materials for Lithium Ion Batteries. *J. Mater. Chem.* **2011**, *21*, 6251−6257.

(20) Zhang, Y.; Sun, W.; Rui, X.; Li, B.; Tan, H. T.; Guo, G.; Madhavi, S.; Zong, Y.; Yan, Q. One-Pot Synthesis of Tunable Crystalline Ni3S4@Amorphous MoS2 Core/Shell Nanospheres for High-Performance Supercapacitors. *Small* **2015**, *11*, 3694−3702.

(21) Worsley, M. A.; Shin, S. J.; Merrill, M. D.; Lenhardt, J.; Nelson, A. J.; Woo, L. Y.; Gash, A. E.; Baumann, T. F.; Orme, C. A. Ultralow Density, Monolithic WS2, MoS2, and MoS2/Graphene Aerogels. *ACS Nano* **2015**, *9*, 4698−4705.

(22) Krishnamoorthy, K.; Veerasubramani, G. K.; Radhakrishnan, S.; Kim, S. J. Supercapacitive Properties of Hydrothermally Synthesized Sphere Like MoS2 Nanostructures. *Mater. Res. Bull.* **2014**, *50*, 499−502.

(23) Huang, K.-J.; Zhang, J.-Z.; Shi, G.-W.; Liu, Y.-M. Hydrothermal Synthesis of Molybdenum Disulfide Nanosheets as Supercapacitors Electrode Material. *Electrochim. Acta* **2014**, *132*, 397−403.

(24) Sun, T.; Li, Z.; Liu, X.; Ma, L.; Wang, J.; Yang, S. Facile Construction of 3D Graphene/MoS2 Composites as Advanced Electrode Materials for Supercapacitors. *J. Power Sources* **2016**, *331*, 180−188.

DOI: 10.1021/acsami.8b09085
ACS Appl. Mater. Interfaces 2018, 10, 35571−35579

(25) Bissett, M. A.; Kinloch, I. A.; Dryfe, R. A. Characterization of MoS2-Graphene Composites for High-Performance Coin Cell Supercapacitors. *ACS Appl. Mater. Interfaces* **2015**, *7*, 17388−17398.
(26) Yu, D.; Dai, L. Self-Assembled Graphene/Carbon Nanotube Hybrid Films for Supercapacitors. *J. Phys. Chem. Lett.* **2010**, *1*, 467−470.
(27) Li, Z.; Wang, J.; Liu, X.; Liu, S.; Ou, J.; Yang, S. Electrostatic Layer-By-Layer Self-Assembly Multilayer Films Based on Graphene and Manganese Dioxide Sheets as Novel Electrode Materials for Supercapacitors. *J. Mater. Chem.* **2011**, *21*, 3397−3403.
(28) Wang, X.; Ding, J.; Yao, S.; Wu, X.; Feng, Q.; Wang, Z.; Geng, B. High Supercapacitor and Adsorption Behaviors of Flower-Like MoS2 Nanostructures. *J. Mater. Chem. A* **2014**, *2*, 15958−15963.
(29) Zhou, W.; Yin, Z.; Du, Y.; Huang, X.; Zeng, Z.; Fan, Z.; Liu, H.; Wang, J.; Zhang, H. Synthesis of Few-Layer MoS2 Nanosheet-Coated TiO2 Nanobelt Heterostructures for Enhanced Photocatalytic Activities. *Small* **2013**, *9*, 140−147.
(30) Wang, L.; Ma, Y.; Yang, M.; Qi, Y. Hierarchical Hollow MoS2 Nanospheres with Enhanced Electrochemical Properties Used as an Electrode in Supercapacitor. *Electrochim. Acta* **2015**, *186*, 391−396.
(31) Hao, C.; Wen, F.; Xiang, J.; Wang, L.; Hou, H.; Su, Z.; Hu, W.; Liu, Z. Controlled Incorporation of Ni(OH)2 Nanoplates into Flowerlike MoS2 Nanosheets for Flexible All-Solid-State Supercapacitors. *Adv. Funct. Mater.* **2014**, *24*, 6700−6707.
(32) Chang, K.; Chen, W. L-Cysteine-Assisted Synthesis of Layered MoS2/Graphene Composites with Excellent Electrochemical Performances for Lithium Ion Batteries. *ACS Nano* **2011**, *5*, 4720−4728.
(33) Sun, P.; Zhang, W.; Hu, X.; Yuan, L.; Huang, Y. Synthesis of Hierarchical MoS2 and Its Electrochemical Performance as an Anode Material for Lithium-Ion Batteries. *J. Mater. Chem. A* **2014**, *2*, 3498−3504.
(34) Zhu, Y. G.; Wang, Y.; Shi, Y.; Huang, Z. X.; Fu, L.; Yang, H. Y. Phase Transformation Induced Capacitance Activation for 3D Graphene-CoO Nanorod Pseudocapacitor. *Adv. Energy Mater.* **2014**, *4*, No. 1301788.
(35) Tang, W.; Peng, L.; Yuan, C.; Wang, J.; Mo, S.; Zhao, C.; Yu, Y.; Min, Y.; Epstein, A. J. Facile Synthesis of 3D Reduced Graphene Oxide and Its Polyaniline Composite for Supercapacitor Application. *Synth. Met.* **2015**, *202*, 140−146.
(36) Brivio, J.; Alexander, D. T.; Kis, A. Ripples and Layers in Ultrathin MoS2 Membranes. *Nano Lett.* **2011**, *11*, 5148−5153.
(37) Rao, C. N.; Matte, H. S.; Maitra, U. Graphene Analogues of Inorganic Layered Materials. *Angew. Chem. Int. Ed.* **2013**, *52*, 13162−13185.
(38) Acerce, M.; Voiry, D.; Chhowalla, M. Metallic 1T Phase MoS2 Nanosheets as Supercapacitor Electrode Materials. *Nat. Nanotechnol.* **2015**, *10*, 313−318.
(39) Zhou, J.; Qin, J.; Zhang, X.; Shi, C.; Liu, E.; Li, J.; Zhao, N.; He, C. 2D Space-Confined Synthesis of Few-Layer MoS2 Anchored on Carbon Nanosheet for Lithium-Ion Battery Anode. *ACS Nano* **2015**, *9*, 3837−3848.
(40) Cunningham, G.; Lotya, M.; McEvoy, N.; Duesberg, G. S.; Vanderschoot, P.; Coleman, J. N. Percolation Scaling in Composites of Exfoliated MoS2 Filled with Nanotubes and Grapheme. *Nanoscale* **2012**, *4*, 6260−6264.
(41) Huang, K. J.; Wang, L.; Liu, Y. J.; Liu, Y. M.; Wang, H. B.; Gan, T.; Wang, L. L. Layered MoS2-Graphene Composites for Supercapacitor Applications with Enhanced Capacitive Performance. *Int. J. Hydrogen Energy* **2013**, *38*, 14027−14034.
(42) Yang, M. H.; Jeong, J. M.; Huh, Y. S.; Choi, B. G. High-Performance Supercapacitor Based on Three-Dimensional MoS2/Graphene Aerogel Composites. *Compos. Sci. Technol.* **2015**, *121*, 123−128.
(43) Patil, S.; Harle, A.; Sathaye, S.; Patil, K. Development of a Novel Method to Grow MoS2 Mono/Few-Layer Films and MoS2-Graphene Hybrid Films for Supercapacitor Applications. *CrystEngComm* **2014**, *16*, 10845−10855.
(44) Zhang, W.-B.; Ma, X.-J.; Kong, L.-B.; Liu, M.-C.; Luo, Y.-C.; Kang, L. Electrochemical Performance of Pseudo-Capacitive Intermetallic Molybdenum Nitride in Acid. *J. Electrochem. Soc.* **2016**, *163*, A1300−A1305.
(45) Karade, S. S.; Dubal, D. P.; Sankapal, B. R. MoS2 Ultrathin Nanoflakes for High Performance Supercapacitors: Room Temperature Chemical Bath Deposition (CBD). *RSC Adv.* **2016**, *6*, 39159−39165.

DOI: 10.1021/acsami.8b09085
ACS Appl. Mater. Interfaces 2018, 10, 35571−35579